Applied Catalysis B: Environmental 99 (2010) 478–484

Contents lists available at ScienceDirect

Applied Catalysis B: Environmental

journal homepage: www.elsevier.com/locate/apcatb

Kinetics of photocatalyzed film removal on self-cleaning surfaces: Simple configurations and useful models

David Ollis*

Chemical and Biomolecular Engineering, North Carolina State University, Raleigh, NC 27695-7905, USA

ARTICLE INFO

Article history:
Available online 3 July 2010

Keywords:
Photocatalysis
Film removal
Self-cleaning surfaces
Direct
Lateral oxidation

ABSTRACT

We develop simple reaction kinetic models for photocatalyzed removal of carbonaceous and sulfur films, and demonstrate their applicability to a common range of deposited film-catalyst configurations studied in the photocatalyst literature:

1. Non-porous photocatalyst, non-porous transparent organic overlayer (stearic, palmitic acids).
2. Porous photocatalyst: transparent organic (stearic acid) in catalyst void volume.
3. Non-porous photocatalyst, non-transparent porous overlayer (sulfur).
4. Non-porous photocatalyst, adjacent organic layer (soot).

In each case, we consider a simple film-catalyst configuration, propose a corresponding one-dimensional physical model for reaction, and compare model results with literature data to evaluate the correspondence between model and experiment. These examples cover both direct and lateral oxidation by photocatalysis. The respective physical and chemical phenomena which determine these rates of film removal include intrinsic catalyst kinetics (1), simultaneous reaction and light attenuation (2), reaction with light absorption by non-transparent organic film (3), and oxidant lateral transport (surface diffusion) (4). In each case, a simple model suffices to represent the key kinetic phenomena. In all cases, the true kinetic order is zero, but the apparent order may be influenced by light absorption (case 2). The apparent rate constant may be influenced by catalyst light absorption (case 2) or overlayer (case 3), or by catalyst–reactant separation (case 4).

1. Introduction

Photocatalyzed film removal via chemical oxidation of continuous or particulate organic films has been explored recently with an interest in "self-cleaning" surfaces [1,2]. The compositions of such organic films have included long chain fatty acids (stearic, oleic, palmitic acids) [3–7], soot [8–12], organic dyes [13,14], bacteria [15] and sulfur [16]. Despite the growing interest in the photocatalyzed oxidation of solid and liquid films, almost no substantial kinetic modeling has appeared.

We now recognize a trio of oxidation mechanisms which are evident in such solid/liquid film oxidation via photocatalysis:

Direct oxidation when the oxidizable film is in direct contact with the photocatalyst.
Lateral oxidation when the oxidizable film is adjacent to the photocatalyst surface, and
Remote oxidation where an air gap separates the catalyst and the oxidizable film.

These three reaction mechanisms occur on appreciably different time scales: fast (direct), intermediate (lateral), and slow (remote) oxidation. These qualities are also reflected in the relative quantum efficiencies for the three processes.

In this paper we derive and test several simple kinetic models for the photocatalyzed removal of carbonaceous and sulfur films. Direct oxidation examples include stearic acid and sulfur; lateral oxidation is shown for soot.

2. Classification of film-catalyst configurations

The observed kinetics of reaction will depend on the interplay of the following variables:

Proximity to the catalyst surface. All the examples below illustrate "direct" oxidation, with the exception of lateral oxidation of soot by diffusing oxidant.

* Tel.: +1 919 515 2329; fax: +1 919 515 3465.
E-mail address: ollis@ncsu.edu.

0926-3373/$ – see front matter © 2010 Elsevier B.V. All rights reserved.
doi:10.1016/j.apcatb.2010.06.029

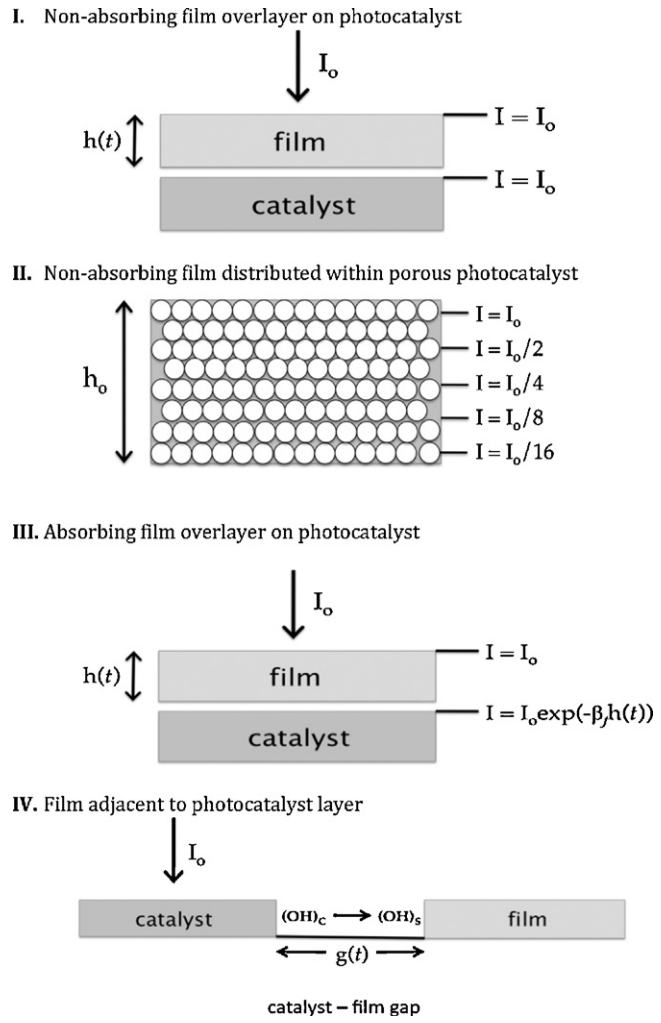

Fig. 1. Film–photocatalyst configurations. Case 1: non-absorbing film overlayer on photocatalyst; case 2: non-absorbing film distributed within porous photocatalyst; case 3: absorbing film overlayer on photocatalyst; case 4: film adjacent to photocatalyst layer.

Porosity: solid, microporous and macro-porous titania layers have been studied, and we distinguish below examples where the film to be oxidized is strictly above the non-porous or porous titania layers, or is within the void structure of the porous photocatalyst. *Intensity*: For material deposited on top of the photocatalyst (and not within it), the intensity reaching the catalyst surface may pass through a transparent coating (stearic and oleic acids) or an absorptive layer (soot, sulfur). In these latter cases, light absorption by the reactant layer must be included in the kinetic model, as we have previously shown for soot oxidation [11,12]. For reaction occurring within an illuminated porous titania layer, the intensity profile influences the local apparent rate constant, as noted earlier for oxidation of vapor phase oxygenates in a powder layer photocatalyst reactor [17].

Given these various circumstances, we propose a set of idealized photocatalyst-film configurations and demonstrate their utility for the models discussed below. These configurations are shown in Fig. 1.

For each configuration we utilize one or more literature examples to provide experimental data, then develop a simple kinetic model, evaluate its parameters, and compare model with data, Given the relative paucity of information to date for photocatalyzed oxidation (PCO) of porous or non-porous organic and sulfur

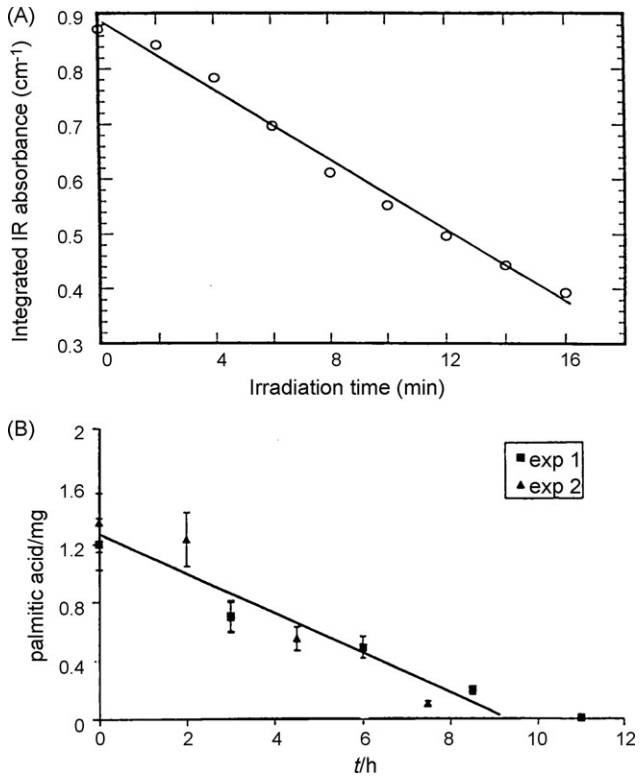

Fig. 2. Removal of fatty acids layers by direct photocatalyzed oxidation. (A) Stearic acid IR absorbance vs. irradiation time (Paz et al. [4]; reprinted by permission of JMR Publishing) and (B) palmitic acid mass (mg) vs. time (Romeas et al. [6]; reprinted by permission of Royal Society of Chemistry). Lines: zero order fit to data.

films, these models are suggestive and simple. Further mechanistic understanding will doubtless lead to more structured models. For the present moment, these remarkably simple models appear to suffice, as we now demonstrate.

3. Model development and parameter evaluation

3.1. Case 1: Non-porous photocatalyst—non-porous overlayers

Early photocatalytic oxidation of films of long chain carboxylic acids was demonstrated by Sitkiewicz and Heller [3], Romeas et al. [6], Puzenat and Pichat [5]. Allain et al. [7], and Mills et al. [8] Data from [4] following the infrared absorbance of –CH2– and CH3– stretching frequencies for stearic acid, and GC determinations of remaining palmitic acid [6] appears in Fig. 2a and b, respectively. In both cases, these multilayer carboxylic acid films appear to be non-porous, and exhibit diminution of film thickness which is zero order in reactant concentration.

3.2. Case 1 model

Here a simple picture of oxygen activation (e.g., as •OH radicals) at the catalyst surface is followed by reaction to release CO_2 continually. The organic layer thins continually (Fig. 3). Assuming no mass transfer limitation by oxygen, the reaction rate is given by:

$$\text{Rate} = -k_o \quad (\text{mol/cm}^2\text{-min})$$

The film mass per unit surface area is density Ω (g/cm^3) times thickness h (cm). A mass balance requires that the time varying film thickness $h(t)$ follows the form:

$$\Omega(\text{mol/cm}^3)\left(\frac{dh}{dt}\right) = -k_o \quad (\text{mol/cm}^2\text{-min})$$

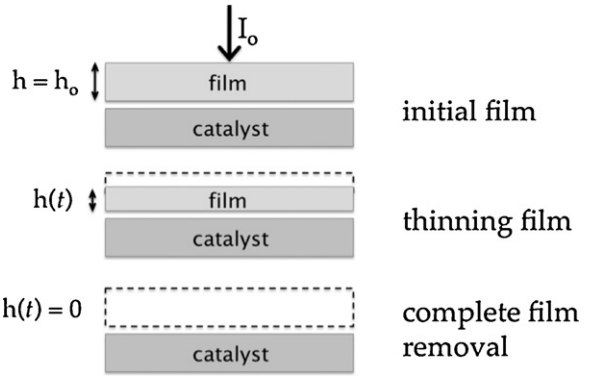

Fig. 3. Evolution of non-absorbing, organic overlayer thickness vs. time.

For initial film thickness $h(t=0)=h_o$, integration yields the predicted time dependence:

$$h(t) = h_o - \frac{k_o t}{\Omega} \quad (1)$$

Multiplication by the total film area A gives the zero order law for total film mass loss rate:

$$M(t) = M_o - \frac{Ak_o t}{\Omega} \quad (2)$$

For this first example of a strongly adherent, non-absorbing overlayer, a zero order rate law for illumination passing through a non-absorbing organic overlayer works well. For these thin films, the rate of oxygen diffusion through the organic layers is assumed to be rapid vs. the stoichiometric demand, consistent with the observed zero order of reaction, independent of overlayer conversion (thickness).

3.3. Case 2: porous photocatalyst layer; void space contains "film" of stearic acid multilayers

Allain et al. [7] synthesized mesoporous titania–silica nanocomposite films to explore the influence of film porosity on photocatalyst performance. The resultant preparations had strongly differing mesopore volumes, as shown in Table 1.

These authors deposited stearic acid films on the composite photocatalysts, citing the procedure of Sitkiewicz and Heller [3]. However, for mesoporous photocatalysts, their monitored 2923 cm^{-1} IR band led to apparent first order behavior shown in Fig. 4, rather than the zero order expected from the earlier stearic acid results of Paz et al. [4] and palmitic acid GC data of Romeas et al. [6].

We propose for an explanation the distribution of reactant stearic acid within the pore structure of the mesoporous composite photocatalyst as indicated in Fig. 5. If we consider the decreasing photocatalytic rate constant with depth into the photocatalyst [17], the reactant will appear to have a different reactivity within each layer of depth. The apparent kinetic behavior of all residing reactant will be a "lumped" version of the individual layers, and will lead to a kinetic order disguise, as we now illustrate. If the top layer has a zero order rate constant of k_o, then we imagine a next layer of reactivity $k_o/2$, a third of $k_o/4$, etc as in each successive layer the absorption by photocatalyst has reduced the intensity by one half. This multilayer model is a useful discrete approximation to continuous variation of k_o due to Beer's law influence on intensity with depth into the catalyst layer.

Table 1
Mesopore and micropore volumes fractions of titania–silica layers [7].

F_v (mesopore)		F_v (micropore)	
cm^3/g	vol%	cm^3/g	vol%
0.2 (d = 5 nm)	39	0.05 (d > 2 nm)	9
0.04 (d > 2 nm)	5	0.005 (d < 2 nm)	4

F, fractional volume as pores.

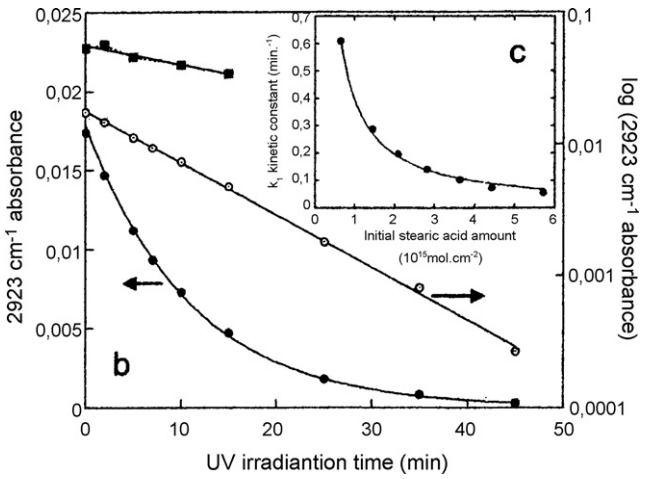

Fig. 4. Removal of stearic acid films from mixed titania–silica photocatalyst layers (Allain et al. [7]; reprinted with permission) (solid circles: absorbance vs. time; open circles: log (absorbance) vs. time. Inset: apparent first order rate constant vs. initial stearic acid amount).

3.4. Case 2 model

Consider reaction in successive layers: each successive layer has a rate constant equal to half that of the layer above it. Then, for a zero order rate constant k_o operating under the illumination at the

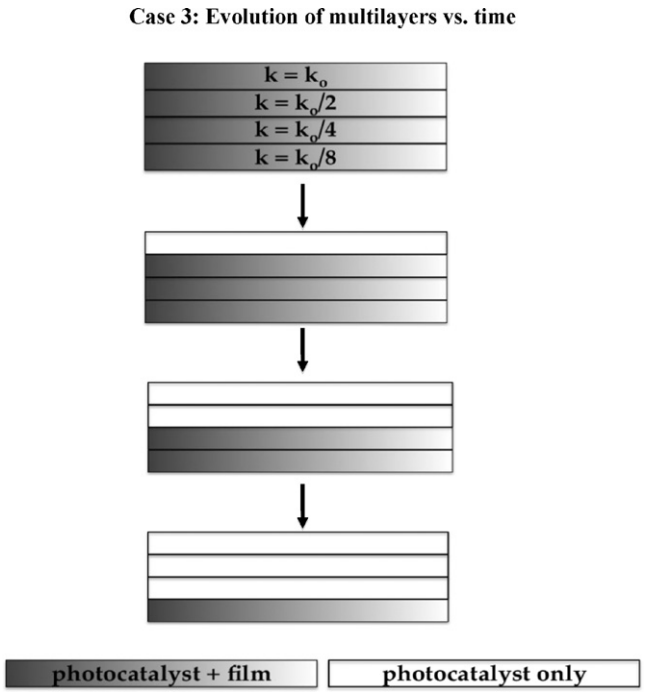

Fig. 5. Configuation case 2: evolution of stearic acid filled porous photocatalyst multilayers vs. time.

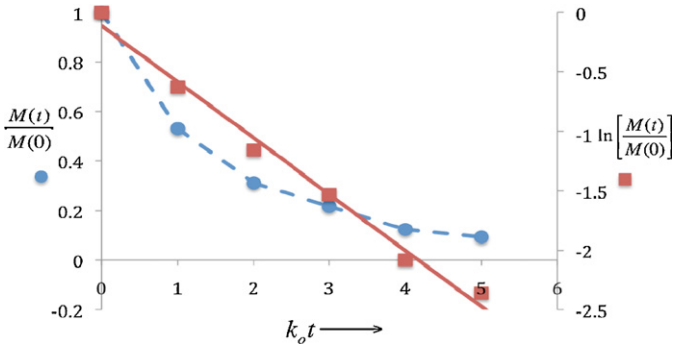

Fig. 6. Stearic acid photocatalyzed oxidation in porous titania–silica films. Filled circles: normalized mass ($M(t)/M(0)$ vs. time; filled squares: ln(normalized mass) vs. time. Linear semilog plot indicates apparent first order reaction.
All data from Fig. 4 (Allain et al. [7]).

surface and mass M/layer,

$$\begin{aligned}&\text{Layer 1}: M_1 = M - k_o t\\ &\text{Layer 2}: M_2 = M - k_o t/2\\ &\text{Layer 3} M_3 = M - k_o t/4\\ &\text{Layer 4}: M_4 = M - k_o t/8\\ &\text{Layer 5}: M_5 = M - k_o t/16\end{aligned} \quad (3)$$

The collective performance of these layers is an approximate representation of intensity which varies exponentially with catalyst depth. The zero order dependence in each layer means that at the end of appropriate intervals of time, the remaining topmost layer will be exhausted and the number of remaining layers is reduced by one. We sum the contributions within the appropriate time regimes to obtain the total mass remaining M_T at any time:

$$\begin{aligned}&0 < t < M/k_o \quad M_T = 5M - k_o t(1 + 1/2 + 1/4 + 1/8 + 1/16)\\ &Mk_o < t < 2M/k_o \quad M_T = 4M - k_o t(1/2 + 1/4 + 1/8 + 1/16)\\ &2\,Mk_o < t < 4\,M/k_o \quad M_T = 3M - k_o t(1/4 + 1/8 + 1/16)\\ &4Mk_o < t < 8\,M/k_o \quad M_T = 2\,M - k_o t(1/8 + 1/16)\\ &8\,Mk_o < t < 16\,M/k_o \quad M_T = 1\,M - k_o t(1/16)\end{aligned} \quad (4)$$

A plot of the total remaining reactant (stearic acid) $M(t)$ appears in Fig. 6. The plot of total mass $M_T(t)$ vs. time gives an apparent concave curve, indicating an apparent positive reaction order. The corresponding semilog plot of $\ln(M_T(t))$ vs. time t produces an apparent straight line. Thus this system in which different volumes possess different zero order rate constants will appear to follow a reaction of first order, i.e., apparent order higher than the true kinetic value. This variation in rate constant with depth can thus rationalize the results of Allain et al. (Fig. 4).

3.5. Combination case 1 and case 2—stearic acid

Mills et al. [8] explored the photocatalyzed destruction of stearic acid layers over two forms of photocatalyst: Activ™ glass comprised of titania films of ca. 15 nm thickness, heat treated at 615 °C, and a porous titania film of ca. 90 ± 10 nm thickness prepared by spin-drying deposition of a 5% (w/v) suspensions of Degussa P25 titania. The latter catalyst consists of 30 μm crystallites firmly attached to others to produce 0.1 μm aggregates, yielding a particulate film with both intra-aggregate and inter-aggregate porosity. Their results in Fig. 7a show a zero order degradation for Activ™ film, and a positive order for the P25 thicker film.

We address this apparent discrepancy in the Fig. 7a data by replotting the Degussa P25 results in semilog form (Fig. 7b) which shows that the data follows an apparent firsts order behavior through the first 85% conversion. We suggest therefore that the thin layer of TiO_2 on Active™ glass represents a non-porous surface, in the sense of Fig. 1a, while the thicker 90 nm porous film is

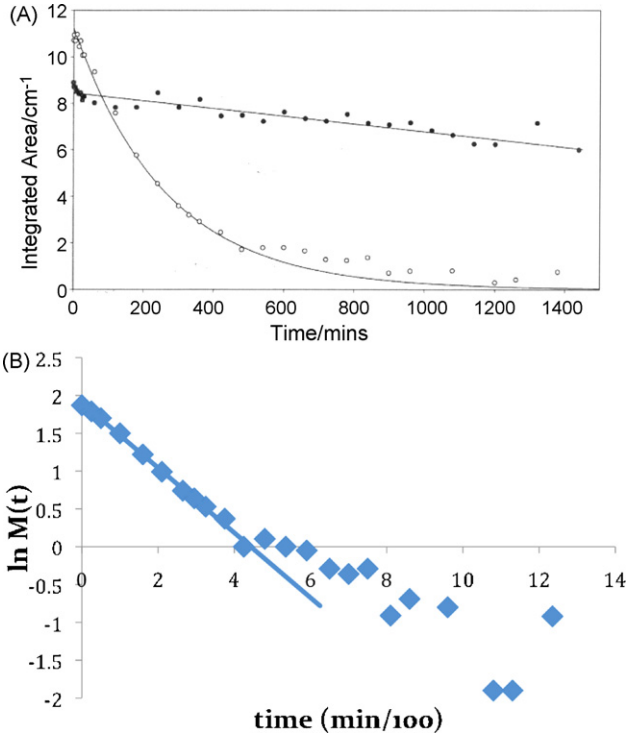

Fig. 7. Stearic acid photocatalyzed oxidation on (A) non-porous ActivTM glass and (B) porous Degussa P25 agglomerate films. (Mills et al. [8]; reprinted by permission.)

our second case (Fig. 1b). As these data are from the same lab and measured with the same instruments and procedures, we conclude that these changes in apparent reaction order are real, and they corroborate our interpretation of the work by Paz et al. [4], Romeas et al. [6] and Allain et al. [7].

3.6. Case 3: non-porous photocatalyst; porous (sulfur) overlayer

Photocatalyzed oxidation of elemental sulfur presents an example of an absorbing, solid film overlayer, deposited by dip coating titania-coated slides in solutions of sulfur dissolved in carbon disulfide, then drying to remove solvent. The resulting samples (Fig. 8) show that "typically 4×10^{-5} g/cm^2 of sulfur were deposited onto the titania films". Mills et al. [16] estimated "the thickness of the sulfur layer as 2.8 μm, comprising particles, typically 260 nm in diameter, but with some ranging in size from 60 to 500 nm. "This

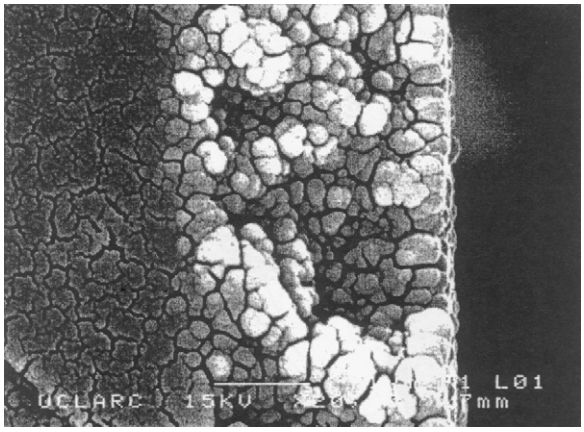

Fig. 8. Amorphous sulfur layer on titania thick film: electron micrograph. Lighter color: sulfur overlayer; darker color: titania sol–gel film (20,000× magnification) (Mills et al. [16], reprinted by permission).

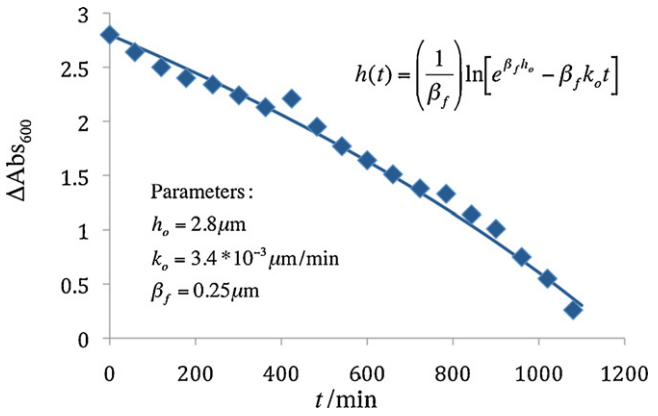

Fig. 9. Photocatalyzed removal of solid, porous sulfur overlayer from thick titania film: diamonds—data of Mills et al. [16]; curve: fitted form of Eq. (8), text.

image also shows that both the darker, underlying titania layer and the lighter, top-coat of amorphous sulfur are very porous.

The overall reaction followed was sulfur oxidation under UVA or UVC illumination. The former was shown to be due exclusively to photocatalysis; the latter almost fully to direct photolytic attack of the sulfur which is highly absorbing in the UVC range. For the former, the photon absorbance of the sulfur film was moderate, and no direct photochemistry of the solid sulfur film was observed.

The film shown in Fig. 8 is adherent yet porous. As reaction proceeds, we may anticipate a zero order reaction as suggested by Mills et al. [16]. However, the curvature of the UVA data plotted as absorbance change vs. time in Fig. 9 requires an explanation, since it indicates that the rate of reaction change over time. As the authors demonstrated a 96% recovery of sulfur, no major intermediate is anticipated, so we assume the simple elementary kinetics of Eq. (5)

$$S(s) + O_2(g) \rightarrow (UVA, TiO_2) \rightarrow SO_2(g) \quad (5)$$

Consider the one-dimensional model of Fig. 10, for which incident UVA is absorbed by TiO_2 after traversing the solid sulfur layer. We assume reaction occurs only at the titania–sulfur film interface, since the photographs provide no evidence of sulfur deposition within the titania. Taking a Beer's law decline of intensity in the sulfur layer, and assuming no mass transfer influence for provision of $O_2(g)$ (and $H_2O(v)$, if needed) by diffusion through the porous film, the change in sulfur layer thickness with time is given by Eq. (5):

$$\frac{dh}{dt} = -k(h) = -k_o \exp -\beta h \quad (6)$$

where β is the absorption coefficient (cm^{-1}) of sulfur (S) and k_o is the zero order rate constant as $h \rightarrow 0$.

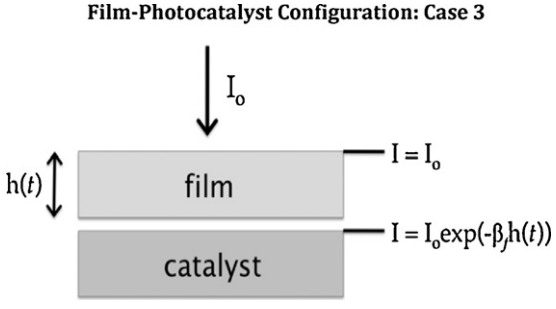

Fig. 10. Configuration case 3: photocatalyzed removal of absorbing overlayer from photocatalyst surface.

Integration gives the value of $h(t)$ for all times, Eq. (7):

$$h(t) = \left(\frac{1}{\beta}\right) \ln[\exp(\beta h_o) - \beta k_o t] \quad (7)$$

Zero order interfacial reaction proceeds with a rate constant which slowly increases with time as the thinning sulfur layer allow greater UVA light flux to reach the TiO_2 surface. We earlier showed that the same phenomenon could explain the curious reaction kinetics observed for the photocatalyzed removal of soot overlayers from near UV illuminated TiO_2 surfaces [10,11].

The sulfur layer is consumed when $h(t) = 0$, or, in terms of Eq. (7), when

$$\exp(\beta h_o) - \beta k_o t = 1.0 \quad (8)$$

We evaluate the parameters h_o, k_o, and β as follows: $h_o = 2.8\ \mu m$ (given, Fig. 8); $k_o = dh/dt$ (evaluated from Fig. 9 at $t = 1130$ min, i.e. as $h \rightarrow 0$) $= 3.4 \times 10^{-3}\ \mu m/min$. $\beta = 0.25\ \mu m$ (=2500 cm^{-1}) from Eq. (8) and h_o, k_o values.

With h_o given and k_o and β evaluated from the predicted slope ($dh/dt = -k_o$) and layer thickness ($h = 0$) at $t = 1130$ min (see Fig. 9), we compare the entire calculated curve $h(t)$ with Mills et al. experimental data [15] for the interval $t = 0 - 1130$ min and find excellent agreement.(Fig. 9).

We conclude that the porous sulfur film deposited directly on the porous TiO_2 layer follows behavior expected for "direct" photocatalyzed oxidation of S on TiO_2. We note that if the sulfur film preparation method had also yielded deposition within the porous titania layer, a pseudo-first order contribution similar to the organic film kinetics discussed earlier would also have been observed. No such indication is found in the microscope photographs (Fig. 8). Apparently the carbon disulfide solution of sulfur did not wet the pore volume of the TiO_2 layer, and the subsequent solvent evaporation procedure yielded sulfur deposited only on the external surface of the titania layer.

3.7. Case 4: lateral oxidation of soot by illuminated TiO_2 film [9]

For a lateral oxidation example, we explore the oxidation of soot by patterned surfaces consisting of TiO_2 "stripes" patterned on a glass surface, followed by uniform deposition of a subsequent soot layer on exposed titania and glass surfaces. Fig. 11a [9]. Direct oxidation of the original overlayer of soot on titania occurs in a relatively short time (32 h, 2 μm thickness, 65 nm/h).) Following exhaustion of this direct overlayer, lateral oxidation of the adjacent soot layer commences, creating a growing gap $g(t)$ between the edges of the TiO_2 "striped" photocatalyst and the receding soot layer (Fig. 11b and c). Scanning electron microscopy images show that this gap grows nearly linearly over time (Fig. 12, data). The approximate slope up to 50 h is (40 μm/55 h=) .73 μm/h = 730 nm/h.

The movement of this soot "edge" is due to soot gasification by mobile oxidants, likely OH radicals, and perhaps also H_2O_2. The former could react directly with the soot, and the latter may be photolyzed (for wavelengths <300 nm) upon arrival at the soot to give 2 OH radicals when the hydrogen peroxide reaches the target surface.

3.8. Case 4 model

The approximately constant velocity of the receding soot edge strongly suggests that surface diffusion is faster than reaction of OH radicals at the soot edge. TiO_2 photocatalyst quantum yields are usually small, because recombination events typically dominate the fate of the active species. We assume a pseudo-stationary state concentration $(OH)_o$ of OH radicals on the TiO_2 surface. We take a soot edge reaction rate r dependent on the local concentration

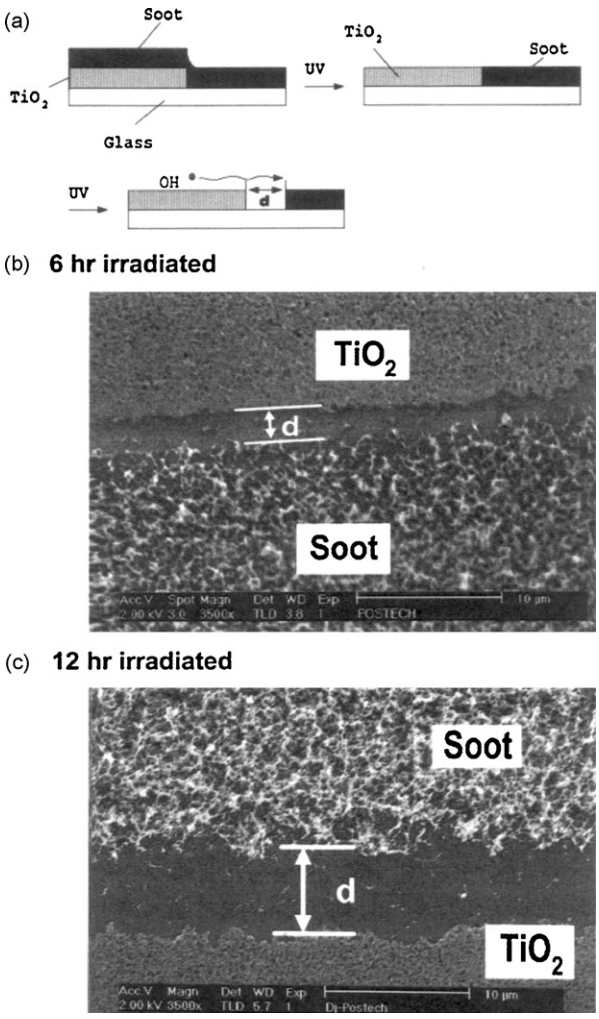

Fig. 11. Removal of adjacent soot layer by lateral photocatalyzed oxidation. (a): Sequence: uniformly deposited initial soot layer; subsequent removal of adlayer soot by direct oxidation; final removal of adjacent soot layer by lateral oxidation. (b and c) Electron micrograph of soot–TiO_2 separation gap d at 6 and 12 h of irradiation, respectively. (Lee and Choi [9]; reprinted by permission.)

of hydroxyl radicals $(OH)_c$ which have moved via surface diffusion across the growing titania-soot gap, $g(t)$, measured fro the edge of the titania layer.

$$r = k(OH)_c \tag{9}$$

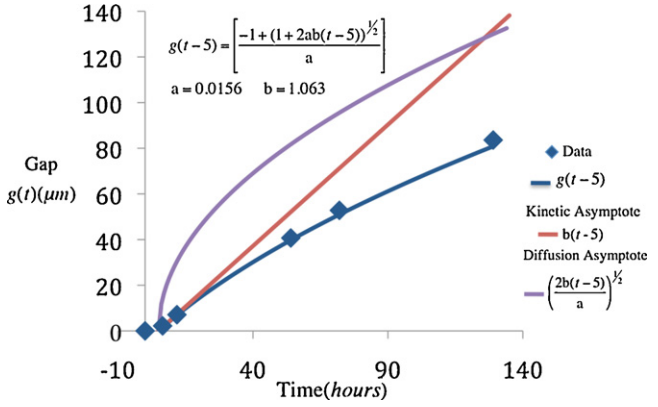

Fig. 12. Soot gap $g(t)$ vs. time. Diamonds—data of Lee and Choi [9]; dark curve: fit of equation $g(t-5)$ (see figure); lighter line: kinetic asymptote $g(t) = [2b(t-5)/a]^{0.5}$; lighter curve: diffusion asymptote $g(t) = b(t-5)$.

at the edge of the receding carbon layer. We then have the serial rate processes of surface diffusion followed by edge reaction:

$$(OH)_o \rightarrow (\text{diffusion}) \rightarrow (OH)_c \rightarrow (\text{reaction}) \rightarrow CO_2$$

At pseudo-steady state, the surface diffusion rate equals the edge reaction rate:

$$\frac{D_s[(OH)_o - (OH)_s]}{g(t)} = k_{cat}(OH)_s \tag{10}$$

where D_s = surface diffusion coefficient (cm^2/s).

Solving for the instantaneous soot edge concentration $(OH)_c$ gives

$$(OH)_c = \frac{(OH)_o}{[\,1 + g(t)k_{cat}/D_s]} \tag{11}$$

where the dimensionless group k_{cat}/D_s is a Damkohler number representing the ratio of maximum reaction rate k_{cat} (OH) to maximum diffusion rate D_c (OH)/g.

The photocatalyzed reaction rate at the soot edge is directly proportional to the edge velocity of the soot layer edge.

$$v = \frac{dg}{dt} = \text{rate} = k_{cat}(OH)_c = \frac{k_{cat}(OH)_o}{[1 + g(t)k_{cat}/D_s]} \tag{12}$$

Thus

$$\left[1 + \frac{g(t)k_{cat}}{D_s}\right] dg = k_{cat}(OH)_o dt$$

Integration gives

$$\left(\frac{k_{cat}}{2D_s}\right) g^2 + g - k_{cat}(OH)_o t = 0$$

so the predicted position $g(t)$ of the moving soot interface is given by

$$g(t) = -1 + \left[\frac{1 + 2k_{cat}/D_s)(k_{cat}(OH)_o)t}{(k_{cat}/D_s)}\right]^{0.5} \tag{13a}$$

Simplifying by defining $a = k_{cat}/D_s$ and $b = k_{cat}\,(OH)_o$, we have

$$g(t) = \frac{-1 + [1 + 2abt]^{0.5}}{a} \tag{13b}$$

This function has asymptotic behaviors for two circumstances of very fast or very slow reaction.

For fast reaction, $abt \gg 1$, and Eq. (13a) simplifies to a diffusion limited case:

$$g(t) = [2D_s(OH)_o t]^{0.5} \quad (\text{surface diffusion limited}) \tag{14a}$$

For slow reaction, $abt \ll 1$, and the second asymptote is

$$g(t) = k_{cat}(OH)_o t \quad (\text{edge reaction limited}) \tag{14b}$$

To compare our model to the experimental data, we first note that a time delay of about 5 h is present before the soot edge begins to move substantially (Fig. 12, data), presumably because some residual carbon on the TiO_2 surface is still consuming OH radicals and thus preventing any substantial (OH) diffusion. With this time shift, we fit our two parameter model to the data at $(t-5) = 49.6$ h, $g = 40$ μm, and $(t-5) = 126$ h, $g = 82$ μm to obtain the values $a = 0.0156$ and $b = 1.063$.

Fig. 12 compares the fitted model, Eq. (13b) to the data for the gap size, $g(t)$, vs. time, and also displays the two limiting, asymptotic cases of reaction limited and diffusion limited rates (Eq. (14a) (14a,b). The full rate form (Eq. (13b)) fits the data well. We conclude that the dual influences of surface reaction and surface diffusion are both involved in the apparent photocatalytic kinetics at nearly all times once the reaction gets underway.

If the surface (OH) radical concentration were known, we could deduce the value of the surface diffusion coefficient. This parameter has proven problematic to measure in other areas of catalysis where radical diffusion is known, e.g., for diffusion of H atoms from Pt metal or to Al_2O_3 or SiO_2 oxide supports [18].

4. Relation of models to the history of catalysis

Heterogeneous catalysis has a long history, and the kinetics of heterogeneous catalysis is filled with examples where reactant transport influences the reaction rate in a manner such that kinetic "disguises" arise, i.e., the apparent kinetic behavior is influenced by both the true reaction kinetics at the catalyst surface and by transport phenomena such as (surface) diffusion [19]. Similarly, light absorption in photocatalyst films (Peral and Ollis [17]) or soot overlayers (Chin et al. [11]) is demonstrated to affect the observed reaction kinetics.

Heterogeneous photocatalysis for self-cleaning surfaces may occur as shown here for circumstances where the film-catalyst contact is superficial (case 1 above), intimate (case 2), or affected by time varying light absorption (case 3) or by surface diffusion (case 4). We expect that inclusion of these transport influences needs consideration for each experimental system examined. Fortunately, the models needed to rationalize the observed kinetic behaviors are simple, as Eqs. (2), (4), (7), and (13a) indicate, so that their use may be relatively convenient for practitioners in the field.

Two other photocatalyst-film circumstances which are not considered here are direct oxidation of soot layers [10,11] and remote oxidation of dyes, soot, etc. These systems appear to be more complex, and are examined in separate papers currently underway.

References

[1] A. Agrios, P. Pichat, J. Appl. Electrochem. 35 (2005) 655.
[2] A. Mills, et al., Res. Chem. Intermed. 31 (2005) 295.
[3] S. Sitkiewitz, A. Heller, New J. Chem. 20 (1996) 233.
[4] Y. Paz, Z. Luo, L. Ragenberg, A. Heller, J. Mater. Res. 10 (1995) 284.
[5] E. Puzenat, P. Pichat, J. Photochem. Photobiol. A 160 (2003) 127.
[6] V. Romeas, P. Pichat, C. Guillard, T. Chopin, G. Lehaut, New J. Chem. 23 (1999) 365.
[7] E. Allain, S. Besson, C. Durand, M. Moreau, T. Gacoin, J.-P. Boilit, Adv. Funct. Mater. 17 (2007) 549.
[8] A. Mills, J. Want, M. Crow, Chemosphere 64 (2006) 1032.
[9] N.C. Lee, W. Choi, J. Phys. Chem. B 106 (2002) 11818.
[10] S.K. Lee, J. McIntyre, A. Mills, J. Photochem. Photobiol. 162 (2004) 203.
[11] P. Chin, G.W. Roberts, D.F. Ollis, Ind. Eng. Res. 46 (2007) 7598.
[12] P. Chin, C. Grant, D.F. Ollis, Appl. Catal. B: Environ. 87 (2009) 220.
[13] A. Julson, D. Ollis, Appl. Catal. B: Environ. 65 (2006) 315.
[14] P. Chin, D. Ollis, Catal. Today 123 (2007) 177.
[15] E.J. Wolfrum, J. Huang, D. Blake, P.C. Manes, Z. Hucag, J. Fiest, W.A. Jacoby, Environ. Sci. Technol. 36 (2002) 3412.
[16] A. Mills, C. Crow, J. Wang, I.P. Parkin, N. Boscher, J. Phys. Chem. C 111 (2007) 5520.
[17] J. Peral, D. Ollis, J. Catal. 136 (1992) 554.
[18] K. Conners, J. Falconer, Chem. Rev. 95 (1995) 759.
[19] O. Levenspiel, Chemical Reaction Engineering, John Wiley & Sons, New York, 1999.